

# Age of Information Analysis in Shared Edge Computing Servers

Federico Chiariotti, *Member, IEEE*

## Abstract

Mobile Edge Computing (MEC) is expected to play a significant role in the development of 6G networks, as new applications such as cooperative driving and eXtended Reality (XR) require both communication and computational resources from the network edge. However, the limited capabilities of edge servers may be strained to perform complex computational tasks within strict latency bounds for multiple clients. In these contexts, both maintaining a low average Age of Information (AoI) and guaranteeing a low Peak AoI (PAoI) even in the worst case may have significant user experience and safety implications. In this work, we investigate a theoretical model of a MEC server, deriving the expected AoI and the PAoI and latency distributions under the First In First Out (FIFO) and Generalized Processor Sharing (GPS) resource allocation policies. We consider both synchronized and unsynchronized systems, and draw insights on the robust design of resource allocation policies from the analytical results.

## Index Terms

Age of Information, Mobile Edge Computing, Generalized Processor Sharing.

## I. INTRODUCTION

One of the promises of the upcoming sixth generation of mobile networks is the union of communication, computation, and sensing as a single service provided by the network [1]: in particular, the rapid developments in Artificial Intelligence (AI) generated a significant demand for low-latency computing power [2], which must be placed at the network edge to avoid long propagation times [3].

Federico Chiariotti (chiariot@dei.unipd.it) is with the Department of Information Engineering, University of Padova, Italy. This work was supported by the European Union under the Italian National Recovery and Resilience Plan of NextGenerationEU, as part of the Young Researchers grant “REDIAL” (SoE0000009).

Cooperative driving is one of the major examples of this trend [4]: automated vehicles require huge neural networks to integrate the data from disparate sensors into a coherent picture, and the emissions from on-board computers may become a significant carbon emitter over the next decade [5]. The efficiency gains from deploying Mobile Edge Computing (MEC), and the possibility of coordinating vehicles in an area [6], has led to a significant amount of research on computational offloading [7] in this context. However, the stringent safety requirements of autonomous vehicles pose a significant challenge: the sensory data from multiple vehicles must be processed and the results of the computation must be distributed within very strict times, often measured in milliseconds. The computational capabilities of edge nodes, or even more mobile platforms such as drones [8], may be hard-pressed to meet these requirements, and system optimization is non-trivial.

Another significant use case for computational offloading is represented by eXtended Reality (XR) [9]: headsets must be battery-powered and light not to encumber the user, but the computational requirements for rendering high-definition virtual scenes, or even overlaying objects on the user's field of view, are significant [10]. The unpredictable nature of XR traffic poses further challenges [11], and the IEEE set a maximum motion-to-photon latency of 20 ms [12] in a recent standard, in order to avoid the insurgence of *cybersickness*, a condition similar to motion sickness caused by a mismatch between visual and proprioceptive sensory inputs.

Computational resource allocation then becomes a significant challenge, which has attracted a significant amount of interest from the research and industrial communities [13]. Generalized Processor Sharing (GPS) is a classical policy [14], [15] that is known to maximize fairness between clients, and is often used in Network Function Virtualization (NFV) and task offloading [16], [17]: it runs all outstanding tasks in parallel by equally splitting the computational resources among them. The opposite policy, First In First Out (FIFO) queuing, allocates all available resources to the client that started service first, providing a faster service once the clients get to the head of the queue but requiring a waiting time if the server is busy. These ubiquitous policies provide a benchmark for any more complex resource allocation mechanisms, and often work extremely well in practical scenarios in terms of latency. However, latency may not capture the full picture in the most relevant use cases [18]: since the processed data are used for control in both the XR and vehicular use cases, the Age of Information (AoI), i.e., the freshness of the information available to the XR user or the self-driving vehicle when they make a decision, is a more compact and meaningful metric [19]. In particular, Peak AoI (PAoI)

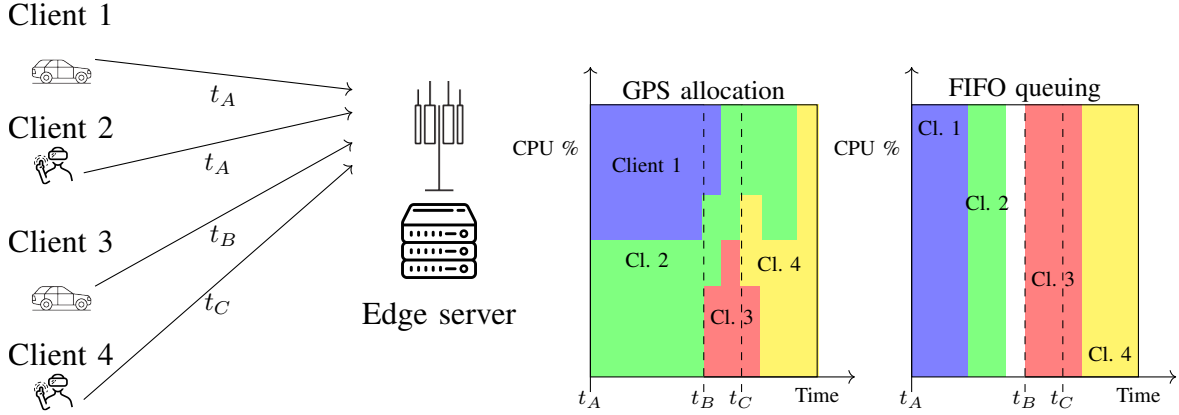


Fig. 1: Depiction of the scenario and of a possible outcome of the two resource sharing policies.

represents an upper bound to the age, and can be used in reliability contexts. These metrics have been extensively used in XR [20], [21] and vehicular [22] use cases.

In this work, we model a scenario such as the one in Fig. 1, in which several clients must share the limited computational resources of a MEC server, and older frames are preempted by new requests from the same client. A possible example of the outcomes of the two opposite policies is also shown in the figure: as described above, GPS divides the available capacity among all active clients, serving them simultaneously at a fraction of the full capacity, while FIFO divides clients in time, giving each one the full capacity of the server, one after the other. We consider the periodic generation of equally complex computational tasks and analyze the distribution of the PAoI, drawing insights on the design of such a system. In particular, our contributions are:

- We analyze the synchronized case, in which users generate frames at the same time, and provide closed-form expressions for the expected AoI and for the Cumulative Density Functions (CDFs) of the computing latency and PAoI for a given client;
- We extend the analysis to the general case in which clients generate frames in batches, under the FIFO and GPS policies, deriving the distributions of the latency and PAoI, as well as the expected AoI;
- We verify the analysis by Monte Carlo simulation<sup>1</sup> and provide design guidelines for MEC systems, analyzing the robustness of the policies to the drift between clients' clocks.

<sup>1</sup>All the code necessary to reproduce the theoretical and Monte Carlo results is publicly available in the following repository: [https://github.com/signetlabdei/aoi\\_edge\\_computing](https://github.com/signetlabdei/aoi_edge_computing)

To the best of our knowledge, this work is the first to theoretically model this scenario, which is extremely relevant for future 6G use cases, and derive the metrics analytically. The rest of the paper is organized as follows: first, Sec. II presents an overview of the state of the art on the subject. The system model is then described in Sec. III, and the analyses for the synchronized and general case are presented in Sec. IV and Sec. V, respectively. Sec. VI then presents the simulations verifying the theoretical calculations, along with the possible design insights deriving from the results, and finally, Sec. VII concludes the paper.

## II. RELATED WORK

As we mentioned in the Introduction, placing computational power as close as possible to users is a major trend in mobile networks [2], enabling almost real-time processing of complex data such as XR frames or vehicular sensory information. The concept of network slicing, i.e., dynamically allocating communication and computational resources based on the Quality of Service (QoS) requirements of users, is another pillar of the evolution of mobile networks into 5G [23] and beyond [24]. Thirdly, the importance of AoI in remote monitoring and control systems has been recognized since the metric's inception [25], but most of the research community's focus was on communications. AoI, and related metrics such as PAoI, have only been applied more recently [26] to edge computing cases, but age-aware slicing policies are crucial for the novel 6G applications mentioned above.

The joint optimization of wireless transmission and computing aspects is a complex task that is often modeled as a Markov Decision Process (MDP) [27] in the relevant literature: as the arrival process to the edge server depends on the access mechanism and wireless channel properties, computing the tandem queue delay and age can require multiple operations, and the complexity of optimization scales accordingly. Considering the worst-case PAoI, in terms of either the violation probability for a specific requirement or a high percentile of the distribution, also increases the complexity of the calculation, but the closed-form PAoI distribution has been derived for some simple systems [19]. The scheduling of updates in this context can lead to better performance [28], but requires the sensor to be able to receive and process feedback, with a higher energy consumption, which may be offset by harvesting energy from the environment [29].

Existing works also consider the effect of different offloading policies between the Edge and Cloud on the AoI [30]: the massive processing capabilities of the Cloud reduce the load, but are partially offset by the higher transmission delay [31]. The choice between offloaded and

local processing is also difficult [32], as the features of the Edge server [8] and the traffic load on it [33] may significantly affect the resulting AoI. This case is also modeled as an MDP to determine optimal scheduling, as stateful offloading decisions manage to keep a lower load and reduce the age [34]. The same models may be used to consider sensing [35] or compression [36] before transmission under different policies, which may also affect access to the shared wireless channel [37].

This type of analysis has been applied to several realistic scenarios. In this case, costs are often defined on the system level, i.e., in terms of operating costs or provider-level QoS metrics. The optimization of Smart City processing is considered in [38], moving computational functions across cells and to the Cloud when necessary, while the radio access using OpenRAN in a vehicular scenario is considered in [39]. Industrial system may also benefit from age-aware policies [40], as the efficiency and energy consumption of control and computation offloading can be improved by considering AoI explicitly [41]. Finally, the AoI in mixed air-ground networks is considered in [42] using game theoretical concepts to model the interactions between individual users and computing-enabled flying base stations.

The research community's interest in freshness-based analysis in mixed communication and computational systems is growing, and some recent works have even started using Age of Processing (AoP) [43] to refer to the age in computational offloading scenarios, to highlight that the system does not just relay and monitor information, but rather needs to actively perform computational transformations [44]. In this context, this work aims at a rigorous analysis of common processor sharing policies, both in terms of average AoI and worst-case PAoI, so as to provide a baseline for future resource slicing algorithms based on more advanced stateful policies.

### III. SYSTEM MODEL

Let us consider a scenario in which  $N$  clients need to share a MEC server's computational capacity for tasks with strict timeliness constraints: possible applications include the rendering of users' different viewpoints in a shared Augmented Reality (AR) environment, or the processing of camera or LIDAR frames generated by autonomous vehicles approaching a crossing. In both cases, each client generates *frames* with a fixed period  $\tau$ . The MEC server then processes those frames; we assume that all frames require a stochastic time to be fully processed, following an exponential distribution with rate  $\mu$ .

In the following, we will consider two different ways of allocating the server's computational capabilities:

- Frames can be processed *sequentially*, following a FIFO queuing model: the client with the oldest frame in service is served first, with the full capabilities of the server allocated exclusively to it;
- Frames can be served *in parallel*, following the well-known GPS policy. In this case, if there are  $X \leq N$  active clients being served, each of their frames will be processed with rate  $\frac{\mu}{X}$ .

In both cases, we consider a preemptive system, i.e., if frame  $i$  from client  $n$  is still being processed after a time  $\tau$ , the  $i + 1$ -th frame from that client supersedes it, so the older frame is discarded and the newer version replaces it in service or in the queue. This assumption is widely used in the AoI literature, and fits systems such as the ones in the examples, as the dynamic nature of the environment makes older data rapidly useless.

In the following, we consider two cases for our optimization:

- In a *synchronized* system, all clients generate frames at the same time: the  $i$ -th frame for client  $n$  is generated at time  $g_{i,n} = i\tau \forall n \in \{1, \dots, N\}$ ;
- In a *batch* system, there are  $B$  batches of clients generating frames at the same time, with an offset  $\nu_b$  from the previous batch. Each batch  $b$  contains  $N_b$  clients, with  $\sum_{b=1}^B N_b = N$ . The  $i$ -th frame from a client  $n$  belonging to batch  $b$ , we then have  $g_{i,n} = i\tau + \sum_{j=2}^b \nu_j$ . Naturally, we also have  $\sum_{b=2}^B \nu_b \leq \tau$ .

The synchronized system is a special case of a batch system with  $B = 1$ ; the opposite extreme, with  $B = N$ , corresponds to a case in which all clients generate frames at different times. In the FIFO scheme, we consider frames arriving simultaneously to be queued randomly every time, as minimal offsets in the clocks of different clients may result in different orderings.

We then define the timeliness metrics we consider in evaluating the two systems: let us consider a single client  $n$ . The  $i$ -th frame from that client is generated at time  $g_{i,n}$ , and the instant in which it is served is denoted as  $s_{i,n}$ , with  $s_{i,n} = +\infty$  if the frame is dropped. The latency  $T_{i,n}$  for the  $i$ -th frame from client  $n$  is then simply given by:

$$T_{i,n} = s_{i,n} - g_{i,n}. \quad (1)$$

We also define the set  $\mathcal{D}_n(t)$ , which includes all the frames from client  $n$  that have been served

by time  $t$ :

$$\mathcal{D}_n(t) = \{i \in \mathbb{N} : s_{i,n} \leq t\}. \quad (2)$$

We can then define the AoI  $\Delta(t)$  as the freshness of the latest received packet at time  $t$ , i.e., the time that has elapsed since its generation:

$$\Delta(t) = t - \max_{i \in \mathcal{D}_n(t)} g_{i,n}. \quad (3)$$

The average AoI  $\bar{\Delta}$  is defined as follows:

$$\bar{\Delta} = \lim_{T \rightarrow \infty} \frac{1}{T} \int_0^T \Delta(t) dt. \quad (4)$$

We can also define the PAAoI  $\Psi_{i,n}$  for each successfully delivered frame:

$$\Psi_{i,n} = s_{i,n} - \max_{j \in \mathcal{D}_n(s_{i,n})} g_{j,n}, \text{ if } \exists T \in \mathbb{R} : s_{i,n} \leq T. \quad (5)$$

We can then use the latency and PAAoI as metrics for the timeliness of the MEC offloading service, computing their complete distribution, as well as the expected AoI  $\bar{\Delta}$ .

#### IV. ANALYSIS: SYNCHRONIZED FRAME GENERATION

We first consider the synchronized case in which frames are generated simultaneously by each client and they all have the same period  $\tau$ . In this case, the MEC server is always fully booked right after a frame is generated. On the other hand, the Probability Mass Function (PMF) of the number of clients right before a new frame is generated,  $X_{\tau-\varepsilon}$ , where  $\varepsilon > 0$  is an infinitesimal value, is given by:

$$p_{X_{\tau-\varepsilon}}(k) = \begin{cases} \frac{\gamma_N(\mu\tau)}{(N-1)!} & \text{if } k = 0; \\ \frac{(\mu\tau)^{N-k} e^{-\mu\tau}}{(N-k)!} & \text{if } k \in \{1, \dots, N\}, \end{cases} \quad (6)$$

where  $\gamma_k(x)$  is the lower incomplete gamma function, which is defined as follows:

$$\gamma_k(x) = \int_0^x e^{-t} t^{k-1} dt. \quad (7)$$

In this special case, there is no prioritization or ordering, as clients are queued randomly, and considering a GPS system or a FIFO queue (which corresponds to a  $D^N/M/1$  in the standard Kendall notation) is then exactly the same thanks to the properties of Poisson processes. As all clients are identical, the success probability  $\sigma$  of a frame from a given client is given by:

$$\sigma = \sum_{k=0}^{N-1} \frac{N-k}{N} p_{X_{\tau-\varepsilon}}(k). \quad (8)$$

Naturally, if  $X_{\tau-\varepsilon} = N$ , no frames have been served by the MEC and no client successfully managed to deliver a frame. As the queue is preemptive, i.e., frames that are not successful before the next frames are generated are substituted by the newer ones, this repeats identically for each frame.

In order to compute the delay experienced by a specific (successful) frame, we can simply consider the fact that, in order for a specific client to have been served by time  $t$ , we need to satisfy two conditions: firstly, at least  $k \geq 1$  frames must have been served by time  $t$ , and secondly, that specific client must be among them. As clients are all identical, the probability of being successful if  $k$  frames have been served is simply  $\frac{k}{N}$ . We can then apply the law of total probability, knowing that served frames follow a Poisson process:

$$P_T(t) = \frac{\gamma_N(\mu t)}{\sigma(N-1)!} + \sum_{k=1}^{N-1} \frac{(\mu t)^k e^{-\mu t}}{N(k-1)!}. \quad (9)$$

Naturally, we have  $P_T(\tau) = 1$ , as this only consider frames successfully delivered by time  $\tau$ . The CDF of the PAoI  $\Psi$  is then given by:

$$P_\Psi(\psi) = \left(1 - (1 - \sigma) \lfloor \frac{\psi - \tau}{\tau} \rfloor (1 - \sigma P_T(\text{mod}(\psi, \tau)))\right) u(\psi - \tau), \quad (10)$$

where  $\text{mod}(m, n)$  is the integer modulo function and  $u(x)$  is the stepwise function, equal to 1 if  $x \geq 0$  and 0 otherwise.

We can also compute the average AoI following the well-known geometric method [45]: if the interval between the generation of two successful frames is  $Y$ , and the latency of the latter is  $T$ , the average AoI  $\bar{\Delta}$  can be computed as:

$$\bar{\Delta} = \frac{1}{\mathbb{E}[Y]} \left( \frac{\mathbb{E}[(T+Y)^2]}{2} - \frac{\mathbb{E}[T^2]}{2} \right) = \frac{\mathbb{E}[Y^2]}{2\mathbb{E}[Y]} + \frac{\mathbb{E}[TY]}{\mathbb{E}[Y]}. \quad (11)$$

As the latency of a frame is independent from what happened before its generation, we know that  $\mathbb{E}[TY] = \mathbb{E}[T] \mathbb{E}[Y]$ , so we get:

$$\bar{\Delta} = \frac{\mathbb{E}[Y^2]}{2\mathbb{E}[Y]} + \mathbb{E}[T]. \quad (12)$$

We know that  $Y$  follows a geometric distribution with probability  $\sigma$ , so that  $\mathbb{E}[Y] = \tau\sigma^{-1}$  and  $\mathbb{E}[Y^2] = \frac{\tau^2(2-\sigma)}{\sigma^2}$ . The expected value of the latency can be computed by integrating  $1 - P_T(t)$ , as given by (9):

$$\mathbb{E}[T] = \int_0^\tau 1 - \frac{\gamma_N(\mu t)}{\sigma(N-1)!} - \sum_{k=1}^{N-1} \frac{(\mu t)^k e^{-\mu t}}{N(k-1)!} dt = -\frac{(1-\sigma)\tau}{\sigma} + \sum_{k=0}^{N-1} \frac{(N-k)\gamma_{k+1}(\mu\tau)}{\mu\sigma N k!}. \quad (13)$$



We can then get the average AoI:

$$\bar{\Delta} = \frac{(2 - \sigma)\tau}{2\sigma} + \mathbb{E}[T] = \frac{\tau}{2} + \sum_{k=0}^{N-1} \frac{(N - k)\gamma_{k+1}(\mu\tau)}{\mu\sigma N k!}. \quad (14)$$

The computational complexity to compute the latency and PAoI CDFs, or the average AoI, is always  $O(N)$ .

## V. ANALYSIS: BATCH FRAME GENERATION

We can now consider the more complex case in which clients are grouped in  $B$  batches. In order to simplify the notation, we group the time offset for each batch  $b$  in vector  $\boldsymbol{\nu}$ , where  $\nu_b$  is the time that occurs between the generation of batches  $b - 1$  and  $b$ , and  $\nu_1 = \tau - \sum_{b=2}^B \nu_b$ .

### A. GPS Operation

We first analyze the GPS system. We can consider the instants immediately before the generation of each batch as the steps of a Markov process, where the state  $\mathbf{s}$  is given by:

- The index  $s_0$  of the next batch;
- The number  $s_b \in \{0, \dots, N_b\}$  of frames from each batch  $b$  that are still in processing immediately before the next batch is generated, i.e., at time  $\nu_{s_0} - \varepsilon$ .

The state vector is then  $\mathbf{s} = (s_0, s_1, \dots, s_B)$ , and the state space of the Markov chain representing the system is  $\{1, \dots, B\} \times \prod_{b=1}^B \{0, \dots, N_b\}$ . In the most extreme case,  $B = N$  and all clients arrive at different times: the size of the Markov chain in that case is  $N2^N$ . For the ease of the reader, we also define subset  $\mathcal{S}_b$  as follows:

$$\mathcal{S}_b = \{\mathbf{s} \in \mathcal{S} : s_0 = b\}. \quad (15)$$

A transition from state  $\mathbf{s}$  to state  $\mathbf{s}'$  is possible if two conditions are met: firstly,  $s'_0 = s_0 + 1$ , as the batch indexes are traversed sequentially.<sup>2</sup> Secondly, aside from batch  $s_0$ , there are no new arrivals, so  $s'_b \leq s_b, \forall b \neq s_0$ . We denote the set of states that are reachable from  $\mathbf{s}$  as  $\mathcal{R}(\mathbf{s})$ :

$$\mathcal{R}(\mathbf{s}) = \{\mathbf{s}' \in \mathcal{S}_{s_0+1} : s'_b \leq s_b, \forall b \notin \{0, s_0\}\}. \quad (16)$$

Additionally, we define the number of active frames right after state  $\mathbf{s}$ ,  $X(\mathbf{s})$ , as follows:

$$X(\mathbf{s}) = N_{s_0} + \sum_{b=1, b \neq s_0}^B s_b. \quad (17)$$

<sup>2</sup>With a slight abuse of notation, we allow batch indices larger than  $B$  in equations, considering  $b > B$  to be equivalent to writing  $\text{mod}(b, B)$  in full. This should be apparent to the reader, and allows for more compact and readable equations.

The value includes all the frames still in processing from other batches, summed to the frames in the new batch that just arrived. We then give the PMF of the number  $C$  of completed frames in interval  $t$ , knowing the initial state and that no new frames are generated before time  $t$ :

$$p_{C|S,T}(c|\mathbf{s}, t) = \begin{cases} \frac{(\mu t)^c e^{-\mu t}}{c!} & \text{if } c < X(\mathbf{s}); \\ \frac{\gamma_{X(\mathbf{s})}(\mu t)}{(X(\mathbf{s})-1)!} & \text{if } c = X(\mathbf{s}). \end{cases} \quad (18)$$

If we consider that  $c$  frames were successfully processed over the interval, the transition probability to the next state follows a multivariate hypergeometric distribution. The transition probability is then given by:

$$P(\mathbf{s}, \mathbf{s}') = \begin{cases} p_{C|S,T} \left( X(\mathbf{s}) - \sum_{b=1}^B s'_b \middle| \mathbf{s}, \nu_{s_0+1} \right) \frac{\binom{N_{s_0}}{N_{s_0}-s'_{s_0}} \prod_{b=1, b \neq s_0}^B \binom{s_b}{s_b-s'_b}}{\binom{X(\mathbf{s})}{X(\mathbf{s})-\sum_{b=1}^B s'_b}}, & \text{if } \mathbf{s}' \in \mathcal{R}(\mathbf{s}); \\ 0, & \text{otherwise.} \end{cases} \quad (19)$$

We can then define a transition matrix  $\mathbf{P}$ , whose entries correspond to the transition probabilities. As all frames are equally likely to be completed, the transition probability is uniform among states that correspond to the same number of events between the two batches. The transition probability matrix over  $m$  steps is simply  $\mathbf{P}^m$ , following the Markov property. The success probability  $\sigma(\mathbf{s})$  for a client generated when in state  $\mathbf{s}$  is then given by:

$$\sigma(\mathbf{s}) = \sum_{\mathbf{s}' \in \mathcal{S}_{s_0}} P^B(\mathbf{s}, \mathbf{s}') \frac{N_{s_0} - s'_{s_0}}{N_{s_0}}. \quad (20)$$

Using the transition probability matrix, we can then easily compute the steady-state probability vector  $\boldsymbol{\pi}$  by using the eigenvalue method. The success probability for a client arriving in batch  $b$  is then given by:

$$\sigma_b = \sum_{\mathbf{s} \in \mathcal{S}_b} \frac{\boldsymbol{\pi}(\mathbf{s}) \sigma(\mathbf{s})}{\sum_{\mathbf{s}' \in \mathcal{S}_b} \boldsymbol{\pi}(\mathbf{s}')}. \quad (21)$$

In order to derive the latency CDF, we first define the probability  $P_{D|X}(t|x)$  of a specific client being served in a time interval  $t$ , if there are  $x$  frames in the system at time 0 and no new frames arrive. This is simply equal to the latency CDF in the synchronized system, as defined in (9).

We also define the batch index  $\beta_b(t)$ , which corresponds to the last batch to be generated before a time  $t$  has passed since batch  $b$ :

$$\beta_b(t) = \inf \left\{ i \in \{b, \dots, B+b-1\} : \sum_{k=b}^i \nu_{k+1} \geq t \right\}. \quad (22)$$

We can also define the batch time  $\tau(b, b')$  as the time between batch  $b$  and the first instance of batch  $b'$ :

$$\tau(b, b') = \begin{cases} \sum_{i=b+1}^{b'} \nu_i, & \text{if } b' > b; \\ \sum_{i=b+1}^{B+b'} \nu_i, & \text{if } b' < b; \\ 0, & \text{if } b = b'. \end{cases} \quad (23)$$

We can then combine (9) and (22) to get the CDF of the latency, considering that  $P^0(\mathbf{s}, \mathbf{s}')$  is the identity matrix and conditioning the distribution on the initial state  $\mathbf{s}$ :

$$P_{T|S}(t|\mathbf{s}) = \sum_{\mathbf{s}' \in \mathcal{S}_{\beta_{s_0}(t)}} \frac{P^{\beta_{s_0}(t)-b}(\mathbf{s}, \mathbf{s}')}{N_{s_0} \sigma(\mathbf{s})} [N_{s_0} - s'_{s_0} (1 - P_{D|S}(t - \tau(b, \beta_{s_0}(t))|\mathbf{s}'))]. \quad (24)$$

The overall latency CDF for a frame in batch  $b$  can be computed using the law of total probability:

$$P_T^{(b)}(t) = \sum_{\mathbf{s} \in \mathcal{S}_b} \frac{\pi(\mathbf{s}) P_{T|S}(t|\mathbf{s})}{\sigma_b \sum_{\mathbf{s}' \in \mathcal{S}_b} \pi(\mathbf{s}')}. \quad (25)$$

Due to the need to multiply matrix  $\mathbf{P}$  to obtain the  $B$ -step transition matrix, the computational complexity of computing the latency CDF is  $O(|\mathcal{S}|^3)$ . In the worst case, i.e., when all clients arrive at different times, this corresponds to  $O(N^3 2^{3N})$ .

We can now compute the PAoI for the system with batch arrivals. In this case, we cannot consider the success probability of successive frames to be independent, as the system is stateful: in order to compute the PAoI, we need to start immediately after a successful transmission. We know that, if we go from state  $\mathbf{s}$  to state  $\mathbf{s}'$ , with  $s_0 = s'_0 = b$ , the success probability for a frame belonging to batch  $b$  is equal to  $\frac{N_{s_0} - s'_{s_0}}{N_{s_0}}$ . By applying Bayes' theorem, we have:

$$P(\mathbf{s}, \mathbf{s}'|D) = \frac{(N_{s_0} - s'_{s_0}) P^B(\mathbf{s}, \mathbf{s}')}{N_{s_0} \sigma(\mathbf{s})}, \quad (26)$$

where  $D$  indicates that a frame generated in state  $\mathbf{s}$  was successfully delivered. We removed the exponent from the notation, as we only consider transitions of  $B$  steps in this case. We can also consider the transition probability in case of failure, denoted as  $\bar{D}$ :

$$P(\mathbf{s}, \mathbf{s}'|\bar{D}) = \frac{s'_{s_0} P^B(\mathbf{s}, \mathbf{s}')}{N_{s_0} (1 - \sigma(\mathbf{s}))}. \quad (27)$$

The transition matrix in the case of failures is then denoted as  $\mathbf{P}_{\bar{D}}$ , and its elements are simply given by:

$$P_{\bar{D}}(\mathbf{s}, \mathbf{s}') = (1 - \sigma(\mathbf{s})) P(\mathbf{s}, \mathbf{s}'|\bar{D}). \quad (28)$$

We also define the transition probability from  $\mathbf{s}$  to  $\mathbf{s}'$  over  $m \geq 1$  steps, where the first frame is the only successful one, which we denote as  $P_{\emptyset}(\mathbf{s}, \mathbf{s}'; m)$ :

$$P_{\emptyset}(\mathbf{s}, \mathbf{s}'; m) = \sum_{\mathbf{s}'' \in \mathcal{S}_b} P(\mathbf{s}, \mathbf{s}'' | D) P_{\bar{D}}^{m-1}(\mathbf{s}'', \mathbf{s}'), \quad (29)$$

where  $P_{\bar{D}}^{m-1}(\mathbf{s}, \mathbf{s}')$  is 1 if  $\mathbf{s} = \mathbf{s}'$  and 0 otherwise. We can then give the CDF of the PAoI:

$$P_{\Psi}^{(b)}(\psi) = u(\psi - \tau) \sum_{\mathbf{s} \in (\mathcal{S}_b)} \frac{\pi(\mathbf{s})\sigma(\mathbf{s}) \left[ 1 - \sum_{\mathbf{s}' \in \mathcal{S}_b} P_{\emptyset}(\mathbf{s}, \mathbf{s}'; \lfloor \frac{\psi}{\tau} \rfloor) (1 - \sigma(\mathbf{s}') P_{T|S}(\text{mod}(\psi, \tau) | \mathbf{s}')) \right]}{\sum_{\mathbf{s}^* \in \mathcal{S}_b} \pi(\mathbf{s}^*)\sigma(\mathbf{s}^*)}. \quad (30)$$

where  $\mathbb{N}^+$  is the set of strictly positive integers. In order to compute the latency distribution, we need a further  $O(\lfloor \frac{\psi}{\tau} \rfloor |\mathcal{S}|^3)$  operations. The complexity of computing the PAoI CDF is then  $O((\lfloor \frac{\psi}{\tau} \rfloor + 1) |\mathcal{S}|^3)$ .

We can finally compute the AoI for the system: as for the synchronized case, we can use the geometric method and obtain the formula in (11). However, computing the values in the formula is significantly harder. The inter-arrival time  $Y$  is an integer multiple of the period  $\tau$ , and its PMF  $p_Y^{(b)}(m\tau)$  is given by:

$$p_Y^{(b)}(m\tau) = \sum_{\mathbf{s} \in (\mathcal{S}_b)} \frac{\pi(\mathbf{s})\sigma(\mathbf{s}) \sum_{\mathbf{s}' \in \mathcal{S}_b} P_{\emptyset}(\mathbf{s}, \mathbf{s}'; m)\sigma(\mathbf{s}')}{\sum_{\mathbf{s}^* \in \mathcal{S}_b} \pi(\mathbf{s}^*)\sigma(\mathbf{s}^*)}. \quad (31)$$

We can expand the transition probability  $P_{\emptyset}(\mathbf{s}, \mathbf{s}'; m)$  to obtain:

$$p_Y^{(b)}(m\tau) = \sum_{\mathbf{s} \in (\mathcal{S}_b)} \frac{\pi(\mathbf{s})\sigma(\mathbf{s})}{\sum_{\mathbf{s}^* \in \mathcal{S}_b} \pi(\mathbf{s}^*)\sigma(\mathbf{s}^*)} \sum_{\mathbf{s}' \in \mathcal{S}_b} \sum_{\mathbf{s}'' \in \mathcal{S}_b} P(\mathbf{s}, \mathbf{s}'' | D) P_{\bar{D}}^{m-1}(\mathbf{s}'', \mathbf{s}')\sigma(\mathbf{s}'). \quad (32)$$

Assuming that  $\mathbf{P}_{\bar{D}}$  is diagonalizable, i.e.,  $\mathbf{P}_{\bar{D}} = \mathbf{V}\mathbf{A}\mathbf{V}^{-1}$ , where  $\mathbf{A}$  is a diagonal matrix (and  $\mathbf{d}$  is the vector representing its diagonal), we can transform the PMF to the following form:

$$p_Y^{(b)}(m\tau) = \sum_{\mathbf{s} \in (\mathcal{S}_b)} \frac{\pi(\mathbf{s})\sigma(\mathbf{s})}{\sum_{\mathbf{s}^* \in \mathcal{S}_b} \pi(\mathbf{s}^*)\sigma(\mathbf{s}^*)} \sum_{\mathbf{s}' \in \mathcal{S}_b} \sum_{\mathbf{s}'' \in \mathcal{S}_b} \sigma(\mathbf{s}') P(\mathbf{s}, \mathbf{s}'' | D) [\mathbf{V}\mathbf{A}^{m-1}\mathbf{V}^{-1}](\mathbf{s}'', \mathbf{s}'). \quad (33)$$

Since  $\mathbf{P}_{\bar{D}}$  is not diagonalizable in the general case, we adopt a perturbation approach [46], adding a small Gaussian noise (in the simulations, we set the variance to  $10^{-6}$ ) to each component of its diagonal by summing a diagonal noise matrix  $\mathbf{W}$  to  $\mathbf{A}$ . This approach [47], which approximates  $\mathbf{A}$  as  $\mathbf{V}(\mathbf{A} + \mathbf{W})\mathbf{V}^{-1} + \mathbf{E}$ , guarantees a small value of  $\|\mathbf{E}\|$  under our conditions. Since we are taking successive powers, the diagonal approximation will have an increasing error, but the probability of having a large number of consecutive failures is relatively small when we operate close to the optimal load, as our numerical results will show. We note that in the synchronized

case, i.e.,  $B = 1$ , the transition matrix has identical rows, resulting in a large error from the naive approximated diagonalization.

We can then compute  $\mathbb{E}[Y]$  as follows:

$$\begin{aligned}
\mathbb{E}[Y] &= \sum_{m=1}^{\infty} m\tau p_Y^{(b)}(m\tau) \\
&= \sum_{m=1}^{\infty} m\tau \sum_{\mathbf{s} \in (\mathcal{S}_b)} \frac{\pi(\mathbf{s})\sigma(\mathbf{s})}{\sum_{\mathbf{s}^* \in \mathcal{S}_b} \pi(\mathbf{s}^*)\sigma(\mathbf{s}^*)} \sum_{\mathbf{s}' \in \mathcal{S}_b} \sum_{\mathbf{s}'' \in \mathcal{S}_b} \sigma(\mathbf{s}') P(\mathbf{s}, \mathbf{s}'' | D) [\mathbf{V}\mathbf{A}^{m-1}\mathbf{V}^{-1}] (\mathbf{s}'', \mathbf{s}') \\
&= \sum_{\mathbf{s} \in (\mathcal{S}_b)} \frac{\pi(\mathbf{s})\sigma(\mathbf{s})\tau}{\sum_{\mathbf{s}^* \in \mathcal{S}_b} \pi(\mathbf{s}^*)\sigma(\mathbf{s}^*)} \sum_{\mathbf{s}' \in \mathcal{S}_b} \sum_{\mathbf{s}'' \in \mathcal{S}_b} \sigma(\mathbf{s}') P(\mathbf{s}, \mathbf{s}'' | D) \left[ \mathbf{V} \left( \sum_{m=1}^{\infty} m\mathbf{A}^{m-1} \right) \mathbf{V}^{-1} \right] (\mathbf{s}'', \mathbf{s}').
\end{aligned} \tag{34}$$

The result of the infinite series is simple, as each element of the diagonal matrix  $\mathbf{A}$  can be computed independently. We can then compute the matrix  $\mathbf{Z}$  that solves the series:

$$Z(i, j) = \begin{cases} \frac{1}{(1-A(i,i))^2}, & \text{if } i = j; \\ 0, & \text{otherwise.} \end{cases} \tag{35}$$

The expected time between two consecutive successful frames is then:

$$\mathbb{E}[Y] = \sum_{\mathbf{s} \in (\mathcal{S}_b)} \frac{\pi(\mathbf{s})\sigma(\mathbf{s})\tau}{\sum_{\mathbf{s}^* \in \mathcal{S}_b} \pi(\mathbf{s}^*)\sigma(\mathbf{s}^*)} \sum_{\mathbf{s}' \in \mathcal{S}_b} \sum_{\mathbf{s}'' \in \mathcal{S}_b} \sigma(\mathbf{s}') P(\mathbf{s}, \mathbf{s}'' | D) [\mathbf{V}\mathbf{U}\mathbf{V}^{-1}] (\mathbf{s}'', \mathbf{s}') \tag{36}$$

We can compute  $\mathbb{E}[Y^2]$  in the same way, defining matrix  $\mathbf{U}$  as follows:

$$U(i, j) = \begin{cases} \frac{1+A(i,i)}{(1-A(i,i))^3}, & \text{if } i = j; \\ 0, & \text{otherwise.} \end{cases} \tag{37}$$

$$\mathbb{E}[Y^2] = \sum_{\mathbf{s} \in (\mathcal{S}_b)} \frac{\pi(\mathbf{s})\sigma(\mathbf{s})\tau^2}{\sum_{\mathbf{s}^* \in \mathcal{S}_b} \pi(\mathbf{s}^*)\sigma(\mathbf{s}^*)} \sum_{\mathbf{s}' \in \mathcal{S}_b} \sum_{\mathbf{s}'' \in \mathcal{S}_b} \sigma(\mathbf{s}') P(\mathbf{s}, \mathbf{s}'' | D) [\mathbf{V}\mathbf{W}\mathbf{V}^{-1}] (\mathbf{s}'', \mathbf{s}') \tag{38}$$

We can then compute  $\mathbb{E}[TY]$ , knowing that  $T$  only depends on the state when the frame is generated. We can then apply the law of total probability, knowing that the final state  $\mathbf{s}'$  is part of the calculation, and get:

$$\mathbb{E}[TY] = \sum_{\mathbf{s} \in (\mathcal{S}_b)} \frac{\pi(\mathbf{s})\sigma(\mathbf{s})\tau}{\sum_{\mathbf{s}^* \in \mathcal{S}_b} \pi(\mathbf{s}^*)\sigma(\mathbf{s}^*)} \sum_{\mathbf{s}' \in \mathcal{S}_b} \sum_{\mathbf{s}'' \in \mathcal{S}_b} \sigma(\mathbf{s}') \mathbb{E}[T | S = \mathbf{s}'] P(\mathbf{s}, \mathbf{s}'' | D) [\mathbf{V}\mathbf{Z}\mathbf{V}^{-1}] (\mathbf{s}'', \mathbf{s}'). \tag{39}$$

We can then finally compute the expected latency, dividing each segment:

$$\begin{aligned}
\mathbb{E}[T|S = \mathbf{s}] &= \int_0^\tau 1 - P_{T|S}(t|\mathbf{s}) dt \\
&= \tau - \int_0^{\nu_{s_0+1}} \frac{P_{D|S}(t|\mathbf{s})}{\sigma(\mathbf{s})} dt + \sum_{b=s_0+1}^{B+s_0-1} \int_0^{\nu_{b+1}} \sum_{\mathbf{s}' \in \mathcal{S}_b} \frac{P^{b-s_0}(\mathbf{s}, \mathbf{s}')}{\sigma(\mathbf{s}) N_{s_0}} (N_{s_0} - s'_0 (1 - P_{D|S}(t|\mathbf{s}')))) dt \\
&= -\frac{(1 - \sigma(\mathbf{s}))\tau}{\sigma(\mathbf{s})} + \sum_{k=0}^{X(\mathbf{s})-1} \frac{(X(\mathbf{s}) - k)\gamma_{k+1}(\mu\nu_{s_0+1})}{\mu X(\mathbf{s})\sigma(\mathbf{s})k!} + \sum_{b=s_0+1}^{B+s_0-1} \sum_{\mathbf{s}' \in \mathcal{S}_b} \frac{s'_0 P^{b-s_0}(\mathbf{s}, \mathbf{s}')}{\mu\sigma(\mathbf{s})N_{s_0}X(\mathbf{s}')} \\
&\quad \times \sum_{k=0}^{X(\mathbf{s}')-1} \frac{(X(\mathbf{s}') - k)\gamma_{k+1}(\mu\nu_{b+1})}{k!}.
\end{aligned} \tag{40}$$

The expected AoI can then be approximated by plugging the results from (36)-(40) into (11).

### B. FIFO Queuing

If we consider a FIFO queue, the state definition can be significantly simplified, as the order of service is fixed: frames from older batches are always served first, with the full rate  $\mu$  of the MEC server. We can then reduce the state to only 2 values:

- The index  $s_0$  of the next batch;
- The number  $s_1 \in \{0, \dots, N\}$  of frames (from any batch) that are still in processing immediately before the next batch is generated, i.e., at time  $\nu_{s_0} - \varepsilon$ .

The state vector is then  $\mathbf{s} = (s_0, s_1)$ , and the state space of the Markov chain representing the system is  $\mathcal{S} = \{0, \dots, B\} \times \{0, \dots, N\}$ . The state space size is  $B(N + 1)$ , and in the most extreme case, each frame arrives at a different time and the state space size is  $N(N + 1)$ . The subset  $\mathcal{S}_b$  has the same meaning as for the GPS case, as defined by (15). We can now define the set of reachable states from state  $\mathbf{s}$ ,  $\mathcal{R}(\mathbf{s})$ :

$$\mathcal{R}(\mathbf{s}) = \{\mathbf{s}' \in \mathcal{S}_{s_0+1} : s'_1 \leq \min(\{s_1 + N_{s_0}, N\})\}. \tag{41}$$

The minimum in the set is due to preemption: if any frames from batch  $s_0$  are still in the system when new frames are generated, they are superseded by their newer version and simply discarded. We can also define  $X(\mathbf{s})$  in a similar way to the version we gave for the GPS system:

$$X(\mathbf{s}) = \min(\{s_1 + N_{s_0}, N\}). \tag{42}$$

The definition of the PMF of the number of events in interval  $\nu(\mathbf{s})$  is then the same as the one given in (18) for the GPS case. The state transition is then simple:

$$P(\mathbf{s}, \mathbf{s}') = \begin{cases} p_{C|S,T}(X(\mathbf{s}) - s'_1 | \mathbf{s}, \nu_{s_0+1}), & \text{if } \mathbf{s}' \in \mathcal{R}(\mathbf{s}); \\ 0, & \text{otherwise.} \end{cases} \quad (43)$$

However, frames in a FIFO  $D^{N_b}/M/1$  queuing system are served one at a time in strict order, instead of sharing the processor. If we consider a frame of batch  $b$ , the frames in the batch will be at the head of the queue, so that the success probability is simple. If the length of the queue after a full period  $\tau$  (i.e., after  $B$  steps of the Markov chain) is lower than  $N - N_b$ , all frames from the batch have been served. Otherwise, only a few (or none) have, and the selection of the served frames within the batch is random:

$$\sigma(\mathbf{s}) = \sum_{s'_1=0}^{N-N_{s_0}} P^B(\mathbf{s}, (s_0, s'_1)) + \sum_{s'_1=N-N_{s_0}+1}^{N-1} P^B(\mathbf{s}, (s_0, s'_1)) \frac{N - s'_1}{N_{s_0}}. \quad (44)$$

As for the GPS case, the stationary state distribution  $\pi$  can be computed using the eigenvector method. We can then follow the same procedure as we did for the GPS case to derive the latency and PAoI distributions, after defining the number  $Q_b(b')$  of frames behind the ones generated in batch  $b$  when the last generated batch is  $b'$ :

$$Q_b(b') = \begin{cases} \sum_{i=b+1}^{b'} N_i, & \text{if } b < b'; \\ \sum_{i=b+1}^B N_i + \sum_{i=1}^{b'} N_i, & \text{if } b > b'; \\ 0, & \text{if } b = b'. \end{cases} \quad (45)$$

The success probability for a frame in batch  $b$  follows (21), using the state success probability from (44). The probability of a frame from batch  $b$  being served by time  $t$ , starting from state  $\mathbf{s}$  at time 0 and with  $t \leq \nu_{s_0}$ , i.e., with no new frames generated between 0 and  $t$ , is:

$$P_{D|S}^{(b)}(t|\mathbf{s}) = \begin{cases} 0, & \text{if } X(\mathbf{s}) \leq Q_b(s_0); \\ \sum_{c=X(\mathbf{s})-Q_b(s_0)}^{X(\mathbf{s})} p_{C|S,T}(c|\mathbf{s}, t) + \sum_{c=[X(\mathbf{s})-Q_b(s_0)-N_b]^++1}^{X(\mathbf{s})-Q_b(s_0)-1} p_{C|S,T}(c|\mathbf{s}, t) \frac{(c-[X(\mathbf{s})-N_b-Q_b(s_0)]^+)}{\min(\{N_b, X(\mathbf{s})-Q_b(s_0)\})}, & \text{otherwise,} \end{cases} \quad (46)$$

where  $[x]^+$  denotes the positive part function, equal to  $x$  if  $x \geq 0$  and 0 otherwise. If  $X(\mathbf{s}) \leq Q_b(s_0)$ , all frames from the batch have already been served. Using the definition of  $\beta_b(t)$

from (22) and the definition of  $\tau(b, b')$  from (23), we can then give the CDF of the latency in the case of a transition from  $\mathbf{s}$  to  $\mathbf{s}'$ :

$$P_{T|S}(t|\mathbf{s}, \mathbf{s}') = \begin{cases} 1, & \text{if } X(\mathbf{s}') \leq Q_{s_0}(\beta_{s_0}(t)); \\ 1 - \frac{(1 - P_{D|S}^{(s_0)}(t - \tau(s_0, \beta_{s_0}(t))|\mathbf{s}'))}{N_{s_0}(X(\mathbf{s}') - Q_{s_0}(\beta_{s_0}(t)))^{-1}}, & \text{if } Q_{s_0}(\beta_{s_0}(t)) < X(\mathbf{s}') < Q_{s_0}(\beta_{s_0}(t)) + N_{s_0}; \\ P_{D|S}^{(s_0)}(t - \tau(s_0, \beta_{s_0}(t))|\mathbf{s}'), & \text{if } X(\mathbf{s}') \geq Q_{s_0}(\beta_{s_0}(t)) + N_{s_0}. \end{cases} \quad (47)$$

We then apply the law of total probability to remove the condition on  $\mathbf{s}'$ :

$$P_{T|S}(t|\mathbf{s}) = (\sigma(\mathbf{s}))^{-1} \sum_{s'_1=0}^N P^{\beta_{s_0}(t)-b}(\mathbf{s}, (\beta_{s_0}(t), s'_1)) P_{T|S}(t|\mathbf{s}, \mathbf{s}'). \quad (48)$$

We can then get the CDF of the latency by applying the law of total probability a second time:

$$P_T^{(b)}(t) = \sum_{\mathbf{s} \in \mathcal{S}_b} \frac{\pi(\mathbf{s})\sigma(\mathbf{s})P_{T|S}(t|\mathbf{s})}{\sum_{\mathbf{s}' \in \mathcal{S}_b} \pi(\mathbf{s}')\sigma(\mathbf{s})}. \quad (49)$$

Following the same procedure that we used for GPS service, we can give the transition probability in case of success. If we go from state  $\mathbf{s}$  to state  $\mathbf{s}'$ , with  $s_0 = s'_0 = b$ , the success probability for a frame belonging to batch  $b$  is equal to  $\min\left(\left\{1, \frac{(N-s'_1)}{N_b}\right\}\right)$ . The conditional transition probability,  $P(\mathbf{s}, \mathbf{s}'|D)$ , can then be computed by applying Bayes' theorem:

$$P(\mathbf{s}, \mathbf{s}'|D) = \begin{cases} \frac{P^B(\mathbf{s}, \mathbf{s}')}{\sigma(\mathbf{s})}, & \text{if } s'_1 \leq N - N_{s_0}; \\ \frac{(N-s'_1)P^B(\mathbf{s}, \mathbf{s}')}{N_{s_0}\sigma(\mathbf{s})}, & \text{otherwise.} \end{cases} \quad (50)$$

We also compute the conditional transition probability in case of failure,  $P(\mathbf{s}, \mathbf{s}'|\bar{D})$ :

$$P(\mathbf{s}, \mathbf{s}'|\bar{D}) = \begin{cases} 0, & \text{if } s'_1 \leq N - N_{s_0}; \\ \frac{(s'_1 - N_{s_0})P^B(\mathbf{s}, \mathbf{s}')}{N_{s_0}(1 - \sigma(\mathbf{s}))}, & \text{otherwise.} \end{cases} \quad (51)$$

The rest of the derivation of the PAoI CDF is the same: the transition matrix in case of a failure  $\mathbf{P}_{\bar{D}}$  is computed as in (28). The transition probability over  $m$  steps, where the first frame is the only successful one, is given by (29), and finally, the PAoI CDF can be obtained by using the FIFO versions of the terms in (30). The complexity of the latency and PAoI calculations is the same as the GPS case, but we note that, as the state space is significantly smaller for most practical cases, the complexity will be correspondingly lower.



In order to derive the expected AoI, we can directly apply (36)-(39) and plug them into (11), while the value of  $\mathbb{E}[T|S = \mathbf{s}]$  is given by:

$$\begin{aligned}
\mathbb{E}[T|S = \mathbf{s}] &= \int_0^\tau 1 - P_{T|S}(t|\mathbf{s}) dt \\
&= \tau - \int_0^{\nu_{s_0+1}} \frac{P_{D|S}(t|\mathbf{s})}{\sigma(\mathbf{s})} dt + \sum_{b=s_0+1}^{B+s_0-1} \int_0^{\nu_{b+1}} \sum_{\mathbf{s}' \in \mathcal{S}_b} \frac{P^{b-s_0}(\mathbf{s}, \mathbf{s}')}{\sigma(\mathbf{s}) N_{s_0}} (N_{s_0} - s'_0 (1 - P_{D|S}(t|\mathbf{s}')) dt \\
&= -\frac{(1 - \sigma(\mathbf{s}))\tau}{\sigma(\mathbf{s})} + \sum_{b=s_0}^{B+s_0-1} \sum_{\mathbf{s}' \in \mathcal{S}_b} \frac{P^{b-s_0}(\mathbf{s}, \mathbf{s}') \min\left(1, \frac{X(\mathbf{s}') - Q_{s_0}(b)}{N_{s_0}}\right)}{\mu\sigma(\mathbf{s})} \\
&\quad \times \sum_{k=0}^{X(\mathbf{s}') - Q_{s_0}(b) - 1} \frac{\min\left(1, \frac{X(\mathbf{s}') - Q_{s_0}(b) - k}{N_{s_0}}\right) \gamma_{k+1}(\mu\nu_{b+1})}{k!}.
\end{aligned} \tag{52}$$

## VI. SIMULATION SETTINGS AND RESULTS

We now verify the correctness of the analysis by Monte Carlo simulation, considering  $L = 10^7$  cycles for each scenario and investigating the main design parameters and choices when dimensioning an edge computing server, namely, the update frequency, the computational power of the server, and the queuing policy and scheduling used to control requests. The parameters for the simulations are specified for each scenario. The units given here are dimensionless, as they are all relative (i.e., if the time unit is 1 ms, the period  $\tau$  is expressed in ms and the service rate  $\mu$  is expressed in frames/ms). Realistic values can be considered for each target application, with no change in the main design considerations.

### A. Synchronized Frame Generation

Firstly, we consider the synchronized frame generation scenario, in which all frames arrive at the same time. In this case, the GPS and FIFO policies have identical results. Fig. 2 shows the latency CDFs for different systems, considering  $\tau = 1$ : firstly, we can note that the Monte Carlo results match the theoretical curves perfectly, confirming the correctness of the derivation. A system with  $N = 10$  and different values of the server computational power  $\mu$  is shown in Fig. 2a, while Fig. 2b shows a system with  $\mu = 5$  and a variable number of clients  $N$ . As expected, a lower number of clients, or a larger computational power, lead to a lower latency and a higher reliability: most of the CDFs do not reach 1, as frames which are not processed after an interval  $\tau$  are discarded and superseded by newer ones from the same clients.

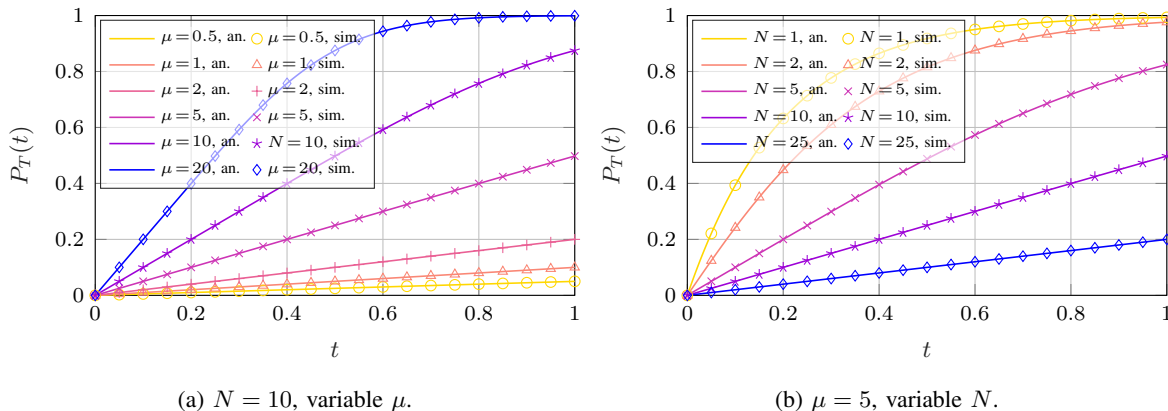


Fig. 2: Latency CDF for synchronized frame generation (frames with a latency larger than  $\tau = 1$  are dropped due to preemption).

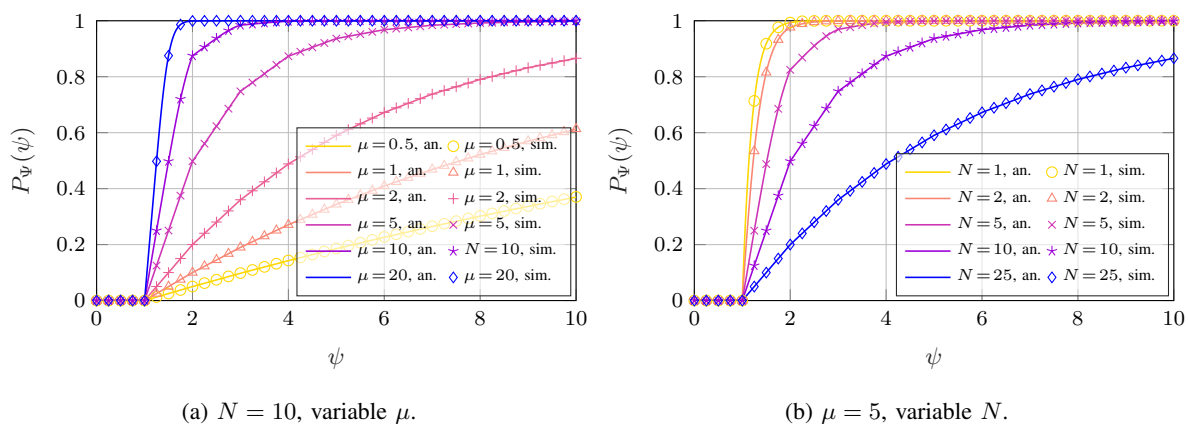


Fig. 3: PAoI CDF for synchronized frame generation with  $\tau = 1$ .

We can also note that the system should be overdimensioned: if  $\mu\tau = N^{-1}$ , i.e., the average load on the server is 1, between 10 and 20% of frames are discarded. We also note that the latency distribution tends to the uniform distribution as the load becomes higher, as would be expected from Poisson departures, while systems with a lighter load have a linear CDF in the first part of the interval, then a lower probability in the second, as the probability of having already served the relevant frame is significantly higher.

We can also look at the PAoI distribution in the same scenarios, shown in Fig. 3: in this case, we can easily see that even relatively underdimensioned systems still have a good worst-case

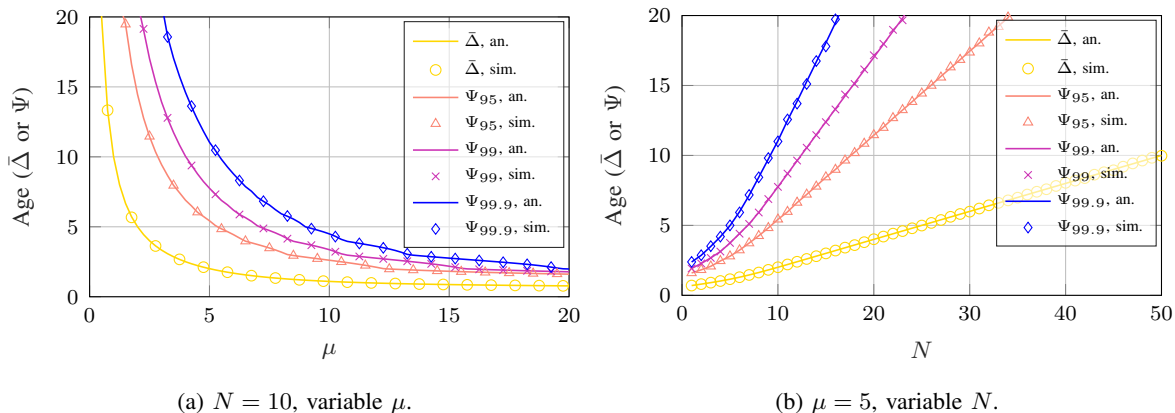


Fig. 4: Average AoI and PAOI percentiles for synchronized frame generation with  $\tau = 1$  as a function of the number of clients  $N$  (with  $\mu = 5$ ) and of the server rate  $\mu$  (with  $N = 10$  clients).

performance. If we consider a system with  $N = 10$  clients, as shown in Fig. 3a, a system with  $\mu = 10$  can guarantee a PAoI lower than 4 with a probability higher than 99%. Even an underdimensioned system with  $\mu = 5$  has a PAoI lower than 4 about 90% of the time. This is due to the resistance of PAoI to discarded frames: even if one or two consecutive frames are lost, a preemptive system which avoids queuing can still deliver fresh information.

We can also consider performance in terms of the average AoI, or the higher percentiles of the PAoI distribution (which we denote for brevity's sake as  $\Psi_p$ , where  $p$  is the percentile), shown in Fig. 4. We can easily see how optimizing the system for the average AoI is much less demanding than worst-case optimization: for a scenario with  $N = 10$  clients, as shown in Fig. 4a, setting  $\mu = 2$  is sufficient to maintain an AoI below 5, while the 99.9th percentile of the PAoI reaches the same value only if  $\mu = 9$ . The same result is clearly visible as  $N$  increases: there is an approximately linear effect for large values of  $N$ , but the slope for higher percentiles is much steeper, as expected.

### B. Batch Frame Generation

We can now consider the more general case of batch frame generation, in which synchronization is not assumed. We first consider the latency CDF as a function of the number of batches, fixing  $N = 8$  and  $\tau = 1$ . Fig. 5 shows the effect of setting different number of (equally sized) batches on the latency CDF: each batch contains  $\frac{N}{B}$  clients, and frames are generated at identical

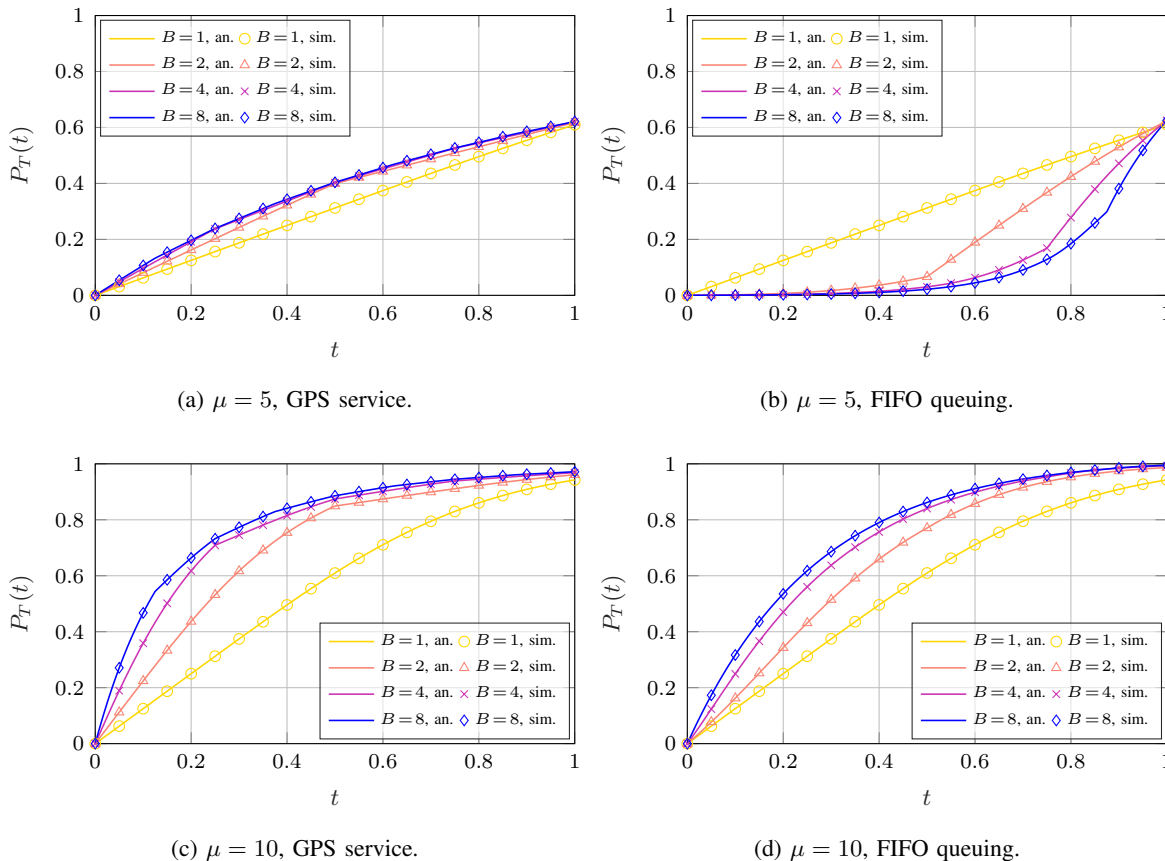


Fig. 5: Latency CDF for different numbers of identical batches with  $\tau = 1$  and  $N = 8$ .

intervals  $\nu_b = \frac{\tau}{B}$ . We can note an interesting difference between the GPS and FIFO systems when  $\mu = 5$ , i.e., when the load is relatively high: in the former, whose latency shown in Fig. 5a, smaller, more spread out batches improve the latency distribution, as each client has a higher chance of having the whole computational power of the server for itself. On the other hand, the FIFO system has a significantly worse performance if we increase the number of batches, as frames are always queued, and their latency distribution shifts toward the right. In the FIFO case, the best latency performance is achieved with  $B = 1$ , which corresponds to the worst case for GPS. However, in both cases, the overall success probability is similar. If we look at the case for GPS. However, in both cases, the overall success probability is similar. If we look at the case with  $\mu = 10$ , i.e., reduce the load by half, the two distributions are much more similar: as shown in Fig. 5c-d, the distribution for the FIFO system is shifted to the right, but the probability of success is higher, as each frame gets a chance to have the server for itself close to the end of the frame period. In this case, using more batches is beneficial for both systems.

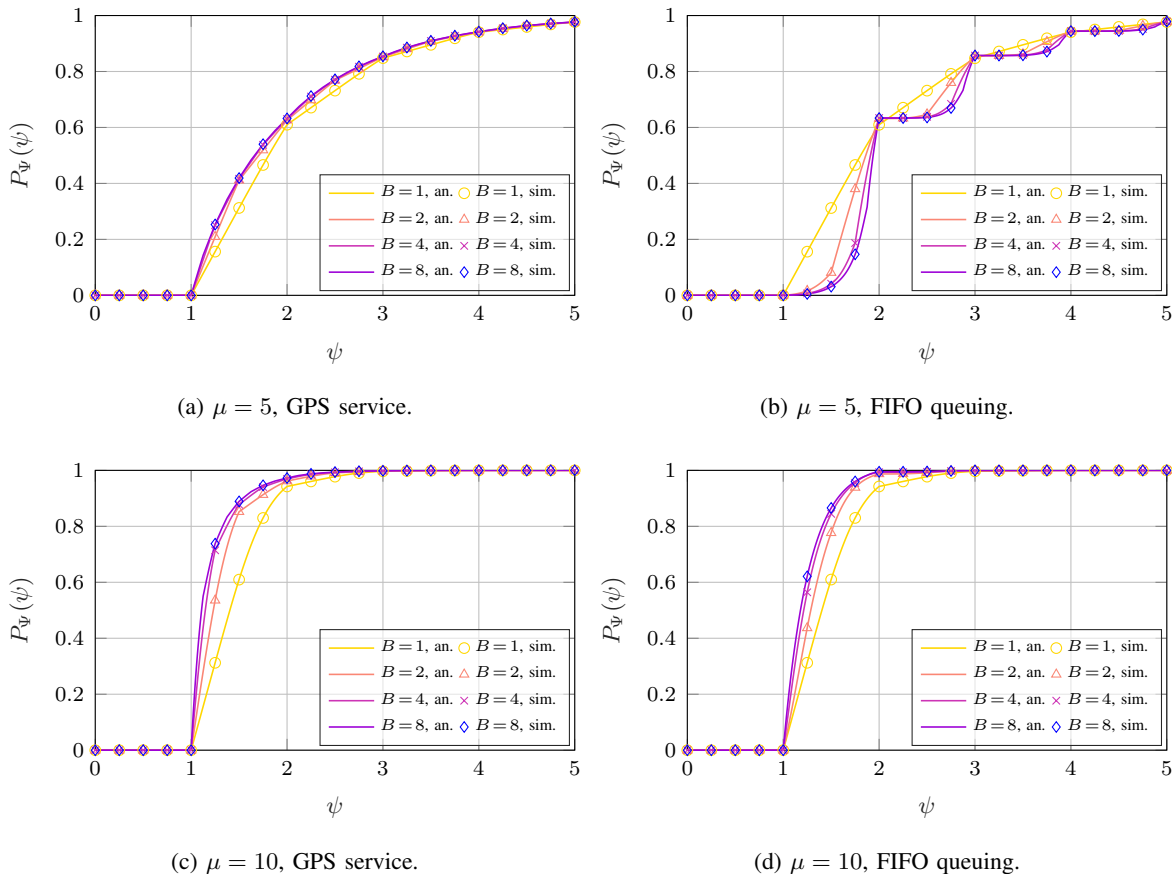


Fig. 6: PAoI CDF for different numbers of identical batches with  $\tau = 1$  and  $N = 8$ .

We can also consider the effect of the batch size on the PAoI, as we show in Fig. 6: we can see an interesting effect in the case with  $\mu = 5$ , as the GPS system shown in Fig. 6a generally performs better, following a mostly concave curve, while the CDF for the FIFO system shown in Fig. 6b has some clear corner points: whenever a period  $\tau$  ends, and the old version of the frame from the client we are considering at the front of the queue is replaced by a new one at the end of the queue, the Probability Density Function (PDF) has a discontinuity. As before, the performance of the synchronized system (i.e.,  $B = 1$ ) is the worst case for GPS and the best case for FIFO. On the other hand, if we set  $\mu = 10$ , as in Fig. 6c-d, the FIFO system manages to have a better worst-case performance, and setting  $B = 8$  is beneficial in both cases.

We can then look at the expected and worst-case age for a fixed scenario, with  $N = 6$ ,  $\mu = 4$ , and individual clients spaced out by a constant period  $\nu$ , as a function of the overall period  $\tau = N\nu$ . We compute the expected AoI and the 95th, 99th, and 99.9th percentiles of

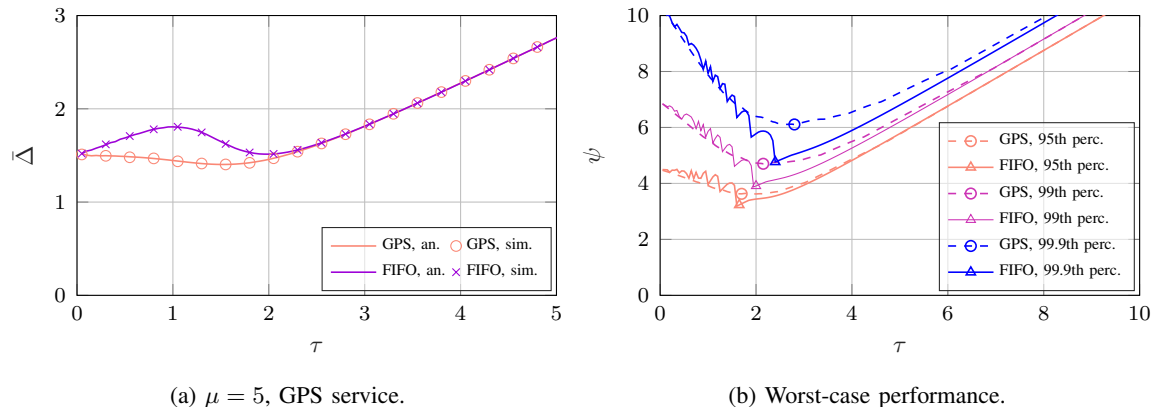


Fig. 7: Worst-case P AoI performance of the GPS and FIFO systems as a function of  $\tau$ , with  $N = 6$ ,  $\mu = 4$ , and  $B = 6$  with identical inter-batch times. The mark indicates the optimal value of  $\tau$  for each percentile and service policy.

the P AoI distribution as a function of the frame period  $\tau$ , as shown in Fig. 7. We first analyze the expected AoI, shown in Fig. 7a: if the value of  $\tau$  is high, i.e., if the load on the system is low, both systems perform equally as well, as we discussed when considering the CDF plots. However, the expected age for the GPS system follows the classic U-shaped curve, while the FIFO system performs worse when the load is higher, with a peak around  $\tau \simeq 1$ . This effect is due to the higher latency that successful frames in a FIFO system experience: while the success probability for a frame is generally similar for the two systems, frames served with GPS often have a shorter latency, reducing the AoI significantly when most frames are successful (i.e., when the latency is a significant component of the AoI). The effect becomes smaller as the frame period gets shorter, i.e., as latency becomes less relevant in determining the AoI.

We can then consider the worst-case performance, shown in Fig. 7b: in general, FIFO systems provide a better performance for intermediate loads, particularly when considering the extreme percentiles, while the performance is similar at both very high and very low loads. Interestingly, the percentiles of the age for the FIFO system show some oscillations for higher loads, instead of decreasing monotonically with  $\tau$  as for the GPS system: this might be due to the discrete nature of arrivals to the system, which results in the staircase-shaped CDF, causing small perturbations to the system to have stronger effects.

Finally, we consider the effect of *drift* on the system: if one client loses synchronization and

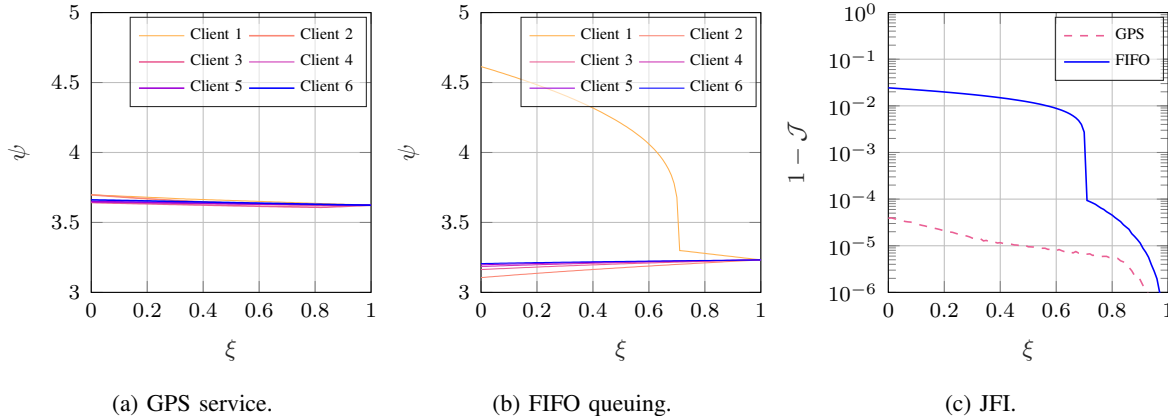


Fig. 8: 95th percentile of the PAoI as a function of the coherence  $\xi$  with  $N = 6$ ,  $\mu = 4$ , and  $B = 6$ . The value of  $\tau$  is optimized for each system.

moves towards the next, while all others transmit at the allotted time, the effect is stronger on the FIFO system than on the GPS one. Considering the system with  $N = 6$ ,  $B = 6$  and equal values of  $\nu$ , i.e., clients arriving with a fixed  $\frac{\tau}{N}$  interval, we suppose that client 1 starts to drift. We then define the coherence value  $\xi \in [0, 1]$ , and consider a scenario in which  $\nu_1 = \xi\nu_3$  and  $\nu_2 = (2 - \xi)\nu_3$ . In other words, client 1 starts transmitting later and getting closer to client 2's allotted time. We then consider the 95th percentile of the PAoI, optimizing  $\tau$  for the case with  $\xi = 1$  (i.e., not considering the drift), and compute the Jain Fairness Index (JFI) of the system, which is defined as:

$$\mathcal{J}(x_1, \dots, x_n) = \frac{(\sum_{i=1}^n x_i)^2}{n \sum_{i=1}^n x_i^2}. \quad (53)$$

Fig. 8 shows what happens in a GPS and FIFO system. In the former, whose performance is shown in Fig. 8a, the 95th percentile PAoI increases slightly for all clients, and client 1 is noticeably underperforming relative to the others when  $\xi$  is close to 0, but the change is minimal. On the other hand, the effect is much more noticeable in the FIFO system, shown in Fig. 8b: since client 1 spends a much shorter time at the head of the queue, its performance becomes much worse, and the PAoI increases by as much as 50%. We can notice this from the JFI plot, shown in Fig. 8c on a logarithmic scale: while the fairness of the GPS system remains almost perfect, the FIFO system's fairness significantly degrades if  $\xi < 0.7$ .

In conclusion, while the FIFO system can generally obtain better worst-case PAoI performance, it is also generally more sensitive to the parameters of the system, and slight timing

inaccuracies can cause some of the clients to have significantly worse outcomes. The higher degree of randomness in the GPS scheme makes it more suitable for systems with a less precise synchronization, as it is generally more robust and can guarantee good performance even when the actual frame generation process is significantly altered.

## VII. CONCLUSION

In this work, we studied the latency and PAoI performance of an edge computing server shared by  $N$  clients, who generate periodic frames that must be processed in a timely fashion. We considered the well-known GPS and FIFO policies, deriving the expected AoI and the latency and PAoI distributions for both. Our analysis yielded some interesting design insights, as the choice between the two service philosophies is non-trivial: in general, a FIFO system can provide better PAoI guarantees in the worst case if the frame generation period  $\tau$  is controllable, but GPS works slightly better for higher levels of system load, can maintain a lower expected AoI, and is generally more robust to perturbations in the arrival process and system parameters.

Future work on the subject may include a more realistic model in the same framework, considering different service time distributions and clients with different needs and frame processing complexity levels. Foresighted policies based on reinforcement learning, which can take the current state of the system into account and dynamically allocate resources to each client, are another interesting avenue of future research, which would bring the analytical results from this study closer to more complex network slicing scenarios, in which performance can only be measured empirically.

## REFERENCES

- [1] Q. Qi, X. Chen, A. Khalili, C. Zhong, Z. Zhang, and D. W. K. Ng, "Integrating sensing, computing, and communication in 6G wireless networks: Design and optimization," *IEEE Transactions on Communications*, vol. 70, no. 9, pp. 6212–6227, Jul. 2022.
- [2] K. B. Letaief, Y. Shi, J. Lu, and J. Lu, "Edge artificial intelligence for 6G: Vision, enabling technologies, and applications," *IEEE Journal on Selected Areas in Communications*, vol. 40, no. 1, pp. 5–36, Nov. 2021.
- [3] "Study on enhancements of edge computing management," 3GPP, Technical Report (TR) 28.814, Release 17, Sep. 2021.
- [4] F. Sun, F. Hou, N. Cheng, M. Wang, H. Zhou, L. Gui, and X. Shen, "Cooperative task scheduling for computation offloading in vehicular Cloud," *IEEE Transactions on Vehicular Technology*, vol. 67, no. 11, pp. 11 049–11 061, Aug. 2018.
- [5] S. Sudhakar, V. Sze, and S. Karaman, "Data centers on wheels: Emissions from computing onboard autonomous vehicles," *IEEE Micro*, vol. 43, no. 1, pp. 29–39, Nov. 2022.
- [6] S. V. Balkus, H. Wang, B. D. Cornet, C. Mahabal, H. Ngo, and H. Fang, "A survey of collaborative machine learning using 5G vehicular communications," *IEEE Communications Surveys & Tutorials*, vol. 24, no. 2, pp. 1280–1303, Feb. 2022.



- [7] L. Liu, C. Chen, Q. Pei, S. Maharjan, and Y. Zhang, "Vehicular edge computing and networking: A survey," *Mobile Networks and Applications*, vol. 26, pp. 1145–1168, Jun. 2021.
- [8] A. Traspadini, M. Giordani, and M. Zorzi, "UAV/HAP-assisted vehicular edge computing in 6G: Where and what to offload?" in *Proceedings of the Joint European Conference on Networks and Communications & 6G Summit (EuCNC/6G Summit)*. IEEE, Jun. 2022, pp. 178–183.
- [9] "Study on XR (Extended Reality) evaluations for NR," 3GPP, Technical Report (TR) 38.838, Release 17, Dec. 2021.
- [10] D. G. Morín, P. Pérez, and A. G. Armada, "Toward the distributed implementation of immersive augmented reality architectures on 5G networks," *IEEE Communications Magazine*, vol. 60, no. 2, pp. 46–52, Feb. 2022.
- [11] ITU-T, "Requirements for mobile edge computing enabled content delivery networks," ITU, Report F.743.10, Nov. 2019.
- [12] IEEE SA, "IEEE Standard for Head-Mounted Display (HMD)-Based Virtual Reality(VR) sickness reduction technology," IEEE, Standard 3079-2020, Sep. 2020.
- [13] J. Zhao, Q. Li, Y. Gong, and K. Zhang, "Computation offloading and resource allocation for Cloud assisted Mobile Edge Computing in vehicular networks," *IEEE Transactions on Vehicular Technology*, vol. 68, no. 8, pp. 7944–7956, Jun. 2019.
- [14] A. Demers, S. Keshav, and S. Shenker, "Analysis and simulation of a fair queueing algorithm," *ACM SIGCOMM Computer Communication Review*, vol. 19, no. 4, pp. 1–12, Aug. 1989.
- [15] A. K. Parekh and R. G. Gallager, "A generalized processor sharing approach to flow control in integrated services networks: The multiple node case," *IEEE/ACM Transactions on Networking*, vol. 2, no. 2, pp. 137–150, Apr. 1994.
- [16] M. Tang and V. W. Wong, "Deep reinforcement learning for task offloading in Mobile Edge Computing systems," *IEEE Transactions on Mobile Computing*, vol. 21, no. 6, pp. 1985–1997, Nov. 2020.
- [17] Y. Zhang and H.-Y. Wei, "Risk-aware Cloud-Edge computing framework for delay-sensitive industrial IoTs," *IEEE Transactions on Network and Service Management*, vol. 18, no. 3, pp. 2659–2671, Jun. 2021.
- [18] P. Popovski, F. Chiariotti, K. Huang, A. E. Kalør, M. Kountouris, N. Pappas, and B. Soret, "A perspective on time toward wireless 6G," *Proceedings of the IEEE*, vol. 110, no. 8, pp. 1116–1146, Jul. 2022.
- [19] F. Chiariotti, O. Vikhrova, B. Soret, and P. Popovski, "Peak age of information distribution for edge computing with wireless links," *IEEE Transactions on Communications*, vol. 69, no. 5, pp. 3176–3191, Feb. 2021.
- [20] C. Chaccour and W. Saad, "On the ruin of Age of Information in Augmented Reality over wireless terahertz (THz) networks," in *Proceedings of the Global Communications Conference (GLOBECOM)*. IEEE, Dec. 2020.
- [21] A. Franco, E. Fitzgerald, B. Landfeldt, and U. Kömer, "Reliability, timeliness and load reduction at the edge for cloud gaming," in *Proceedings of the 38th International Performance Computing and Communications Conference (IPCCC)*. IEEE, Oct. 2019.
- [22] M. K. Abdel-Aziz, S. Samarakoon, C.-F. Liu, M. Bennis, and W. Saad, "Optimized Age of Information tail for Ultra-Reliable Low-Latency Communications in vehicular networks," *IEEE Transactions on Communications*, vol. 68, no. 3, pp. 1911–1924, Dec. 2019.
- [23] S. Zhang, "An overview of network slicing for 5G," *IEEE Wireless Communications*, vol. 26, no. 3, pp. 111–117, Apr. 2019.
- [24] W. Wu, C. Zhou, M. Li, H. Wu, H. Zhou, N. Zhang, X. S. Shen, and W. Zhuang, "AI-native network slicing for 6G networks," *IEEE Wireless Communications*, vol. 29, no. 1, pp. 96–103, Feb. 2022.
- [25] S. Kaul, R. Yates, and M. Gruteser, "Real-time status: How often should one update?" in *Proceedings of the Computer Communications Conference (INFOCOM)*. IEEE, Mar. 2012, pp. 2731–2735.
- [26] Q. Kuang, J. Gong, X. Chen, and X. Ma, "Age-of-information for computation-intensive messages in mobile edge computing," in *Proceedings of the 11th International Conference on Wireless Communications and Signal Processing (WCSP)*. IEEE, Oct. 2019.

- [27] S. Jayanth and R. V. Bhat, "Age of processed information minimization over fading multiple access channels," *IEEE Transactions on Wireless Communications*, vol. 22, no. 3, pp. 1664–1676, Sep. 2022.
- [28] J. Zhu and J. Gong, "Online scheduling of transmission and processing for AoI minimization with edge computing," in *Proceedings of the Conference on Computer Communications Workshops (INFOCOM WKSHPS)*. IEEE, May 2022.
- [29] L. Liu, X. Qin, X. Xu, H. Li, F. R. Yu, and P. Zhang, "Optimizing information freshness in MEC-assisted status update systems with heterogeneous energy harvesting devices," *IEEE Internet of Things Journal*, vol. 8, no. 23, pp. 17 057–17 070, Apr. 2021.
- [30] X. Qin, Y. Li, X. Song, N. Ma, C. Huang, and P. Zhang, "Timeliness of information for computation-intensive status updates in task-oriented communications," *IEEE Journal on Selected Areas in Communications*, vol. 41, no. 3, pp. 623–638, Dec. 2022.
- [31] P. Zou, X. Wei, O. Ozel, T. Lan, and S. Subramaniam, "Timely probabilistic data preprocessing in Mobile Edge Computing," in *Proceedings of the Wireless Communications and Networking Conference (WCNC)*. IEEE, Mar. 2021.
- [32] X. He, S. Wang, X. Wang, S. Xu, and J. Ren, "Age-based scheduling for monitoring and control applications in Mobile Edge Computing systems," in *Proceedings of the Conference on Computer Communications (INFOCOM)*. IEEE, May 2022, pp. 1009–1018.
- [33] H. Li, G. Gong, J. Zhang, H. Zhao, L. Zhou, and J. Wei, "Analysis on age of information in partial computing edge computing systems with multi source-destination pairs," in *Proceedings of the 96th Vehicular Technology Conference (VTC2022-Fall)*. IEEE, Sep. 2022.
- [34] Y. Jiang, J. Liu, I. Humar, M. Chen, S. A. Alqahtani, and M. S. Hossain, "Age of information-based computation offloading and transmission scheduling in Mobile Edge Computing-enabled IoT networks," *IEEE Internet of Things Journal*, Jun. 2023, Early Access.
- [35] Y. Chen, Z. Chang, G. Min, S. Mao, and T. Hämäläinen, "Joint optimization of sensing and computation for status update in Mobile Edge Computing systems," *IEEE Transactions on Wireless Communications*, Mar. 2023, Early Access.
- [36] H. Hu, Y. Dong, Y. Jiang, Q. Chen, and J. Zhang, "On the age of information and energy efficiency in cellular IoT networks with data compression," *IEEE Internet of Things Journal*, vol. 10, no. 6, pp. 5226–5239, Nov. 2022.
- [37] B. Zhou and W. Saad, "Age of information in ultra-dense computation-intensive Internet of Things (IoT) systems," in *Proceedings of the 19th International Symposium on Modeling and Optimization in Mobile, Ad hoc, and Wireless Networks (WiOpt)*. IEEE, Oct. 2021, pp. 1–8.
- [38] N. Modina, R. El Azouzi, F. De Pellegrini, D. S. Menasche, and R. Figueiredo, "Joint traffic offloading and aging control in 5G IoT networks," *IEEE Transactions on Mobile Computing*, 2023, Early Access.
- [39] A. Ndikumana, K. K. Nguyen, and M. Cheriet, "Age of processing-based data offloading for autonomous vehicles in multiRATs Open RAN," *IEEE Transactions on Intelligent Transportation Systems*, vol. 23, no. 11, pp. 21 450–21 464, Jul. 2022.
- [40] X. Xie, H. Wang, and X. Liu, "Scheduling for minimizing the age of information in multi-sensor multi-server Industrial IoT systems," *IEEE Transactions on Industrial Informatics*, Apr. 2023, Early Access.
- [41] J. Huang, H. Gao, S. Wan, and Y. Chen, "Aoi-aware energy control and computation offloading for industrial IoT," *Future Generation Computer Systems*, vol. 139, pp. 29–37, Feb. 2023.
- [42] X. Chen, C. Wu, T. Chen, Z. Liu, H. Zhang, M. Bennis, H. Liu, and Y. Ji, "Information freshness-aware task offloading in air-ground integrated edge computing systems," *IEEE Journal on Selected Areas in Communications*, vol. 40, no. 1, pp. 243–258, Jan. 2022.
- [43] R. Li, Q. Ma, J. Gong, Z. Zhou, and X. Chen, "Age of processing: Age-driven status sampling and processing offloading

- for edge-computing-enabled real-time IoT applications,” *IEEE Internet of Things Journal*, vol. 8, no. 19, pp. 14 471–14 484, Mar. 2021.
- [44] Y. Liu, B. Yang, X. Yang, Y. Wu, and C. Li, “Microservice dynamic migration based on age of service for edge computing,” in *Proceedings of the International Conference on Industrial Technology (ICIT)*. IEEE, Aug. 2022.
- [45] R. D. Yates, Y. Sun, D. R. Brown, S. K. Kaul, E. Modiano, and S. Ulukus, “Age of information: An introduction and survey,” *IEEE Journal on Selected Areas in Communications*, vol. 39, no. 5, pp. 1183–1210, Mar. 2021.
- [46] A. Greenbaum, R.-c. Li, and M. L. Overton, “First-order perturbation theory for eigenvalues and eigenvectors,” *SIAM Review*, vol. 62, no. 2, pp. 463–482, Jun. 2020.
- [47] E. B. Davies, “Approximate diagonalization,” *SIAM Journal on Matrix Analysis and Applications*, vol. 29, no. 4, pp. 1051–1064, Jun. 2008.